X-ray characterization of atomic-layer superlattices

2005 J. Phys. D: Appl. Phys. 38 A147

(http://iopscience.iop.org/0022-3727/38/10A/028)

INSTITUTE OF PHYSICS PUBLISHING JOURNAL OF PHYSICS D: APPLIED PHYSICS
J. Phys. D: Appl. Phys. **38** (2005) A147–A153 doi:10.1088/0022-3727/38/10A/028

X-ray characterization of atomic-layer superlattices

J H Li[1], S C Moss[1], Y Zhang[2], A Mascarenhas[2] and J Bai[3]

[1] Department of Physics and Texas Center for Superconductivity and Advanced Materials, University of Houston, Houston, TX 77204-5005, USA
[2] National Renewable Energy Laboratory, Golden, CO 80401, USA
[3] Oak Ridge National Laboratory, Oak Ridge, TN 37831, USA

Received 1 March 2005
Published 6 May 2005
Online at stacks.iop.org/JPhysD/38/A147

Abstract
We have characterized the structure of AlAs/GaAs atomic-layer superlattices by x-ray diffraction. We show that when the superlattice layers are only a few monolayers (MLs) thick, lateral domains of vertical extent of 1–2 MLs exist. The small layer thickness also magnifies the growth error, leading to periodic compositional stacking faults in the growth direction. As the layer thickness increases, the lateral domain structures tend to behave like interfacial roughness. Growth interruption between successive layers enlarges the lateral domains, but does not remove the vertical stacking faults.

1. Introduction

X-ray scattering, including large-angle diffraction, small-angle reflection, grazing-incidence diffraction, etc, has long been used as a standard technique for the characterization of semiconductor superlattices in which the individual layers are considerably thicker than the unit cell of the constituent materials [1]. Structural information, such as layer thickness, strain, composition and interfacial roughness, can be obtained by analysing and/or theoretically modelling the experimental curves. There is typically a preferred range of superlattice period, Λ, ideal for x-ray analysis, so that a sufficient number of superlattice peaks with an interval $2\pi/\Lambda$ can be recorded. It has been shown that even for the best superlattices grown using advanced techniques, such as molecular beam epitaxy (MBE), an interfacial width of at least a few monolayers (MLs) exists. Conventionally, such interfaces are treated as small perturbations in the scattering theory, which explains, in most cases, the scattering data quite well [1, 2]. However, if the superlattice period is reduced, the contribution of the interfaces becomes larger in the whole structure, and the perturbation theory becomes questionable.

In this paper, we report a structural analysis of superlattices with a period as small as one unit cell using a conventional coplanar x-ray diffraction technique and a kinematic approach. We have measured and analysed the x-ray diffraction patterns of a series of $(AlAs)_n/(GaAs)_n$ atomic-layer superlattices (hereafter n/n superlattices), where n denotes the number of atomic MLs and ranges from 1 to 10. We show that these superlattices contain lateral domain structures and vertical compositional stacking faults (CSF). The effect of growth interruption between neighbouring layers is also discussed.

2. Experimental procedure and results

$(AlAs)_n/(GaAs)_n$ superlattices with $n = 1, 2, 4$ and 10 were grown by MBE on undoped GaAs (001) substrates at a temperature of 450°C and a deposition rate of 0.1 nm s^{-1}. Prior to the superlattice growth, a 300 nm GaAs buffer layer was grown at 650°C. The first set of superlattices was grown without interruption while switching from one material to another. After that, a 1/1 superlattice was grown with an interruption of 10 s after deposition of each material. The samples are about $1.5 \times 1.5\,mm^2$ in size. For the 1/1, 2/2, 4/4 and 10/10 superlattices, 1000, 500, 200 and 100 periods have been deposited, respectively. The x-ray diffraction measurements were performed at beamline X14A of the National Synchrotron Light Source (NSLS) at the Brookhaven National Laboratory. The x-ray energy used was 8.0478 keV. The incident beam slit, located about 30 cm away from the sample, has an aperture of about $0.15 \times 0.15\,mm^2$. On the detector arm, a receiving slit with a $0.2 \times 0.2\,mm^2$ aperture is located about 35 cm from the sample.

For a perfect 1/1 superlattice, the Ga and Al atoms form a typical CuAu–I structure, as shown in figure 1. The structure

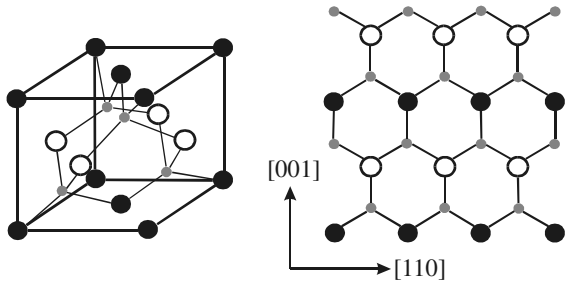

Figure 1. (*a*) Schematic diagram of a unit cell of an ideal (AlAs)1/(GaAs)1 superlattice. The structure is very similar to that of the ordered CuAu–I alloy. (*b*) Projection of the 1/1 superlattice on the [110] lattice plane.

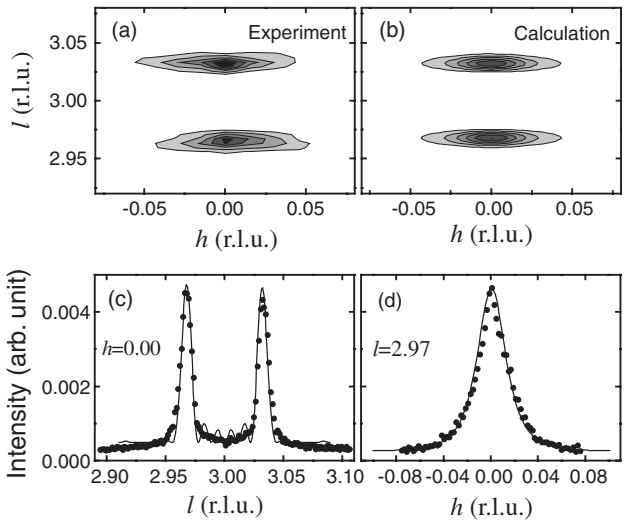

Figure 2. (*a*) Measured and (*b*) calculated x-ray intensity contour maps around the (003) reciprocal lattice point of the 1/1 superlattice. (*c*) l-scan at $h = 0$ and (*d*) h-scan at $l = 2.97$. The dots and line represent the measured and calculated results, respectively.

factor of the (00l) rod of such an ordered structure can be written as

$$F_{00l} = f_{\mathrm{GaAs}} + f_{\mathrm{AlAs}}\mathrm{e}^{\pi i l} = \begin{cases} f_{\mathrm{GaAs}} + f_{\mathrm{AlAs}} & l \text{ is even—fundamental,} \\ f_{\mathrm{GaAs}} - f_{\mathrm{AlAs}} & l \text{ is odd,} \end{cases} \tag{1}$$

where f_{GaAs} and f_{AlAs} denote the structure factors of a GaAs and a AlAs molecule, respectively. An even l corresponds to a fundamental reflection, such as (002) or (004), which contains no superlattice information. An odd l, however, corresponds to a usually forbidden reflection, such as (003), which reflects the contrast between the GaAs and AlAs MLs and thus corresponds to a superlattice reflection.

According to this analysis, we have measured the (003) reflection from the 1/1 superlattice without growth interruption. The result is shown in figure 2(*a*). Surprisingly, we do not see the peak at (003). Rather, we see two split peaks located at (0,0,3 ± 0.033). Moreover, these peaks are considerably broadened along the lateral (110) direction.

Similarly, the structure factor of (00l) reflection of a perfect 2/2 superlattice can be written as

$$F_{00l} = (f_{\mathrm{GaAs}} + f_{\mathrm{AlAs}}\mathrm{e}^{\pi i l})(1 + \mathrm{e}^{2\pi i l}) = \begin{cases} 2(f_{\mathrm{GaAs}} + f_{\mathrm{AlAs}}) & l \text{ is even—fundamental,} \\ 0 & l \text{ is odd,} \\ (f_{\mathrm{GaAs}} - f_{\mathrm{AlAs}})(1 \pm \mathrm{i}) & l = m/2 \text{ and } m \text{ is odd.} \end{cases} \tag{2}$$

Therefore, the superlattice reflections should be those with $l = m/2$ (m is odd). We may also consider the possibility that the two GaAs MLs, as well as the two AlAs MLs, are not identical for some reason. Then equation (2) should be expanded as

$$F_{00l} = (f_{\mathrm{GaAs\text{-}1}} + f_{\mathrm{GaAs\text{-}2}}\mathrm{e}^{\pi i l}) + \mathrm{e}^{2\pi i l}(f_{\mathrm{AlAs\text{-}1}} + f_{\mathrm{AlAs\text{-}2}}\mathrm{e}^{\pi i l}) = \begin{cases} (f_{\mathrm{GaAs\text{-}1}} + f_{\mathrm{GaAs\text{-}2}}) + (f_{\mathrm{AlAs\text{-}1}} + f_{\mathrm{AlAs\text{-}2}}) \\ \quad l \text{ is even—fundamental,} \\ (f_{\mathrm{GaAs\text{-}1}} - f_{\mathrm{GaAs\text{-}2}}) + (f_{\mathrm{AlAs\text{-}1}} - f_{\mathrm{AlAs\text{-}2}}) \\ \quad l \text{ is odd,} \\ (f_{\mathrm{GaAs\text{-}1}} - f_{\mathrm{AlAs\text{-}1}}) \pm \mathrm{i}(f_{\mathrm{GaAs\text{-}2}} - f_{\mathrm{AlAs\text{-}2}}) \\ \quad l = m/2 \text{ and } m \text{ is odd.} \end{cases} \tag{3}$$

This means that if the two MLs of the same material are not identical, we should also be able to see the reflection when l is odd. Therefore, we must look at (00l) reflections with l equals m and $m/2$ (m is odd).

We have measured both the (003) reflection and the (0,0,2.5) and (0,0,3.5) reflections for the 2/2 superlattice. No peak is seen at (003), indicating that the two MLs of GaAs, as well as the two MLs of AlAs, can each be considered identical within the resolution of our experiment. The (0,0,2.5) and (0,0,3.5) reflections, shown in figures 3 and 4, to our surprise, do not appear at the expected positions but shift up or down to (0,0,2.49) and (0,0,3.51), respectively. Again, these peaks are broadened along the lateral (110) direction.

For the 4/4 superlattice, if we consider the possibility that each ML of the same material is different from the others, the structure factor can then be written as

$$F_{00l} = (f_{\mathrm{GaAs\text{-}1,2}} + f_{\mathrm{GaAs\text{-}3,4}}\mathrm{e}^{2\pi i l}) + \mathrm{e}^{4\pi i l}(f_{\mathrm{AlAs\text{-}1,2}} + f_{\mathrm{AlAs\text{-}3,4}}\mathrm{e}^{2\pi i l}) = \begin{cases} (f_{\mathrm{GaAs\text{-}1,2}} + f_{\mathrm{GaAs\text{-}3,4}}) + (f_{\mathrm{AlAs\text{-}1,2}} + f_{\mathrm{AlAs\text{-}3,4}}) \\ \quad l \text{ is even—fundamental,} \\ (f_{\mathrm{GaAs\text{-}1,2}} - f_{\mathrm{GaAs\text{-}3,4}}) + (f_{\mathrm{AlAs\text{-}1,2}} - f_{\mathrm{AlAs\text{-}3,4}}) \\ \quad l = m/2 \text{ and } m \text{ is odd,} \\ (f_{\mathrm{GaAs\text{-}1,2}} \pm \mathrm{i}f_{\mathrm{GaAs\text{-}3,4}}) - (f_{\mathrm{AlAs\text{-}1,2}} \pm \mathrm{i}f_{\mathrm{AlAs\text{-}3,4}}) \\ \quad l = m/4, \\ (f_{\mathrm{GaAs\text{-}1}} - f_{\mathrm{GaAs\text{-}2}}) + (f_{\mathrm{GaAs\text{-}3}} - f_{\mathrm{GaAs\text{-}4}}) \\ \quad +(f_{\mathrm{AlAs\text{-}1}} - f_{\mathrm{AlAs\text{-}2}}) + (f_{\mathrm{AlAs\text{-}3}} - f_{\mathrm{AlAs\text{-}4}}) \\ \quad\quad l \text{ is odd,} \end{cases} \tag{4}$$

where $f_{R\text{-}1,2} = f_{R\text{-}1} + f_{R\text{-}2}\mathrm{e}^{\pi i l}$ and $f_{R\text{-}3,4} = f_{R\text{-}3} + f_{R\text{-}4}\mathrm{e}^{\pi i l}$ (R = GaAs or AlAs). We see that when l is odd, the (00l) peak reflects the contrast between the two neighbouring MLs of the same material. Such reflections have not been observed experimentally, indicating that there is no observable difference between layers 1 and 2, as well as between layers 3 and 4. However, we did observe the (0,0,m/2) (m is odd) reflections, as shown in figure 5(*a*), suggesting that there is an appreciable difference between the layers 1, 2 and layers 3, 4 of the same material. This, together with the result from the

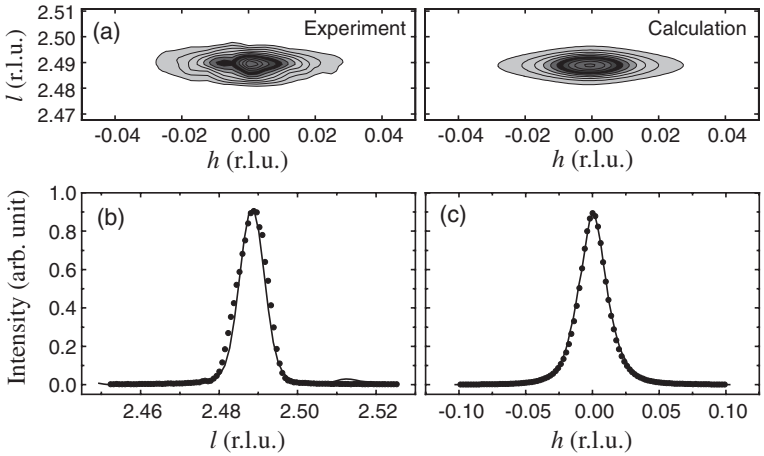

Figure 3. (*a*) Measured and (*b*) calculated x-ray intensity contour maps around the (0,0,2.5) reciprocal lattice point of the 2/2 superlattice. (*c*) *l*-scan at $h = 0$ and (*d*) *h*-scan at $l = 2.49$. The dots and line represent the measured and calculated results, respectively.

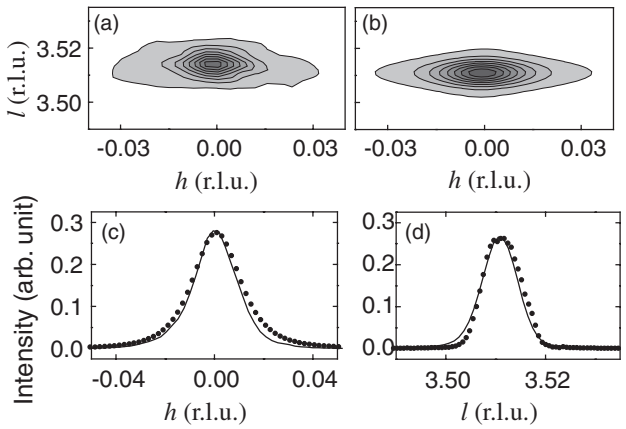

Figure 4. (*a*) Measured and (*b*) calculated x-ray intensity contour maps around the (0,0,3.5) reciprocal lattice point of the 2/2 superlattice. (*c*) *l*-scan at $h = 0$ and (*d*) *h*-scan at $l = 3.51$. The dots and line represent the measured and calculated results, respectively.

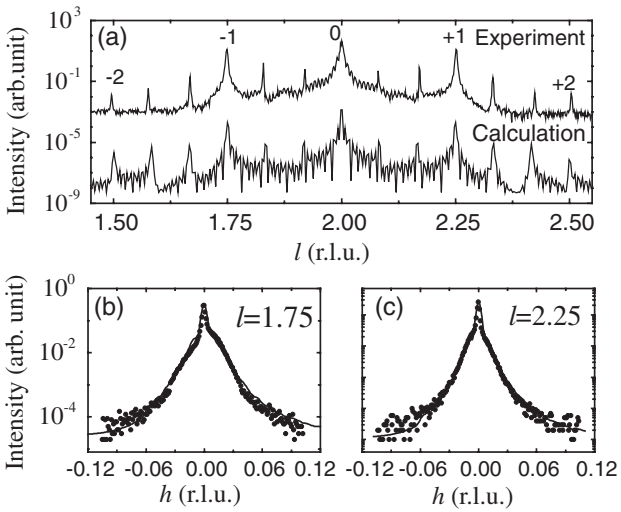

Figure 5. (*a*) *l*-scan in the vicinity of the (002) reciprocal lattice point of the 4/4 superlattce. Upper and lower curves are from measurements and calculations, respectively. The regular superlattice satellites are indexed. (*b*) and (*c*) *h*-scans at $l = 1.75$ and 2.25, respectively. The dots and line represent the measured and calculated results, respectively.

2/2 superlattice, indicates that the perturbation is about 2 MLs in the growth direction.

The unusual features observed from the 4/4 superlattice include: (1) two extra peaks between the neighbouring superlattice peaks; (2) unlike the 1/1 and 2/2 superlattice, where uniform peak broadening is seen along the lateral direction, the transverse scans from the 4/4 structure across the superlattice peaks contain two components, a narrow one superimposed on a broad one, as shown in figures 5(*b*) and (*c*).

The results from the 10/10 superlattice are similarly predicted. Only expected superlattice peaks with an interval of $2\pi/t_p$ (t_p is the thickness of one period) are observed, as shown in figure 6. Moreover, the transverse scan across the superlattice peak is considerably narrow, as shown in figure 7.

Finally, we measured the (003) reflection from the 1/1 superlattice with 10 s growth interruption. The result is shown in figure 8. Compared with the 1/1 superlattice without growth interruption, the peak splitting remains the same, but the lateral peak width is reduced considerably. Moreover, the split peaks have shoulders, indicating the structure is not uniform.

3. Theoretical approach

Although the x-ray results presented earlier deviate from the expected ideal superlattice structure, it is clear that an ordered structure has been successfully grown even for the smallest 1/1 superlattice because otherwise the observed x-ray peaks would not appear. However, there must be modifications to the expected layer-by-layer structure to account for the deviations. Since the AlAs/GaAs system is nearly lattice matched and the layer thickness is very small, extended crystalline defects, such as misfit dislocations and positional stacking faults, are not expected. However, it is quite possible that occupational defects exist: namely, the two group-III elements, Ga and Al, may switch lattice sites. Such occupational defects have been observed in many spontaneously ordered metallic alloys, such as CuAu, etc and semiconductor alloy films, such as InGaP/GaAs (001), etc although the origins for these two types

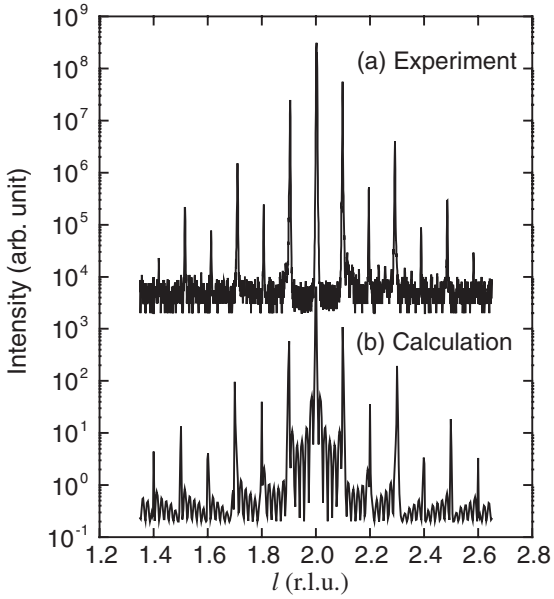

Figure 6. l-scan in the vicinity of the (002) reciprocal lattice point of the 10/10 superlattce. Curve (a) is the measurement and curve (b) is our calculation.

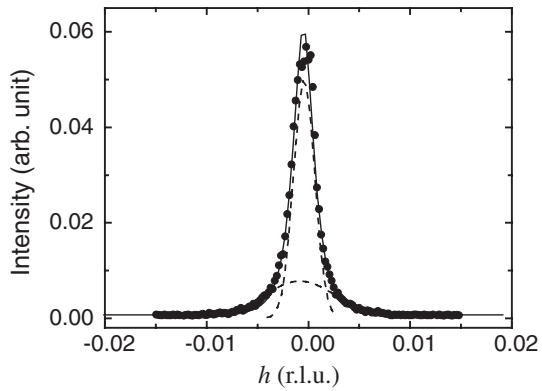

Figure 7. h-scan at $l = 2.10$ taken from the 10/10 superlattice. The peak is narrow, but a broad component arising from the interfacial domain structure can still be resolved, as shown by the dashed line.

of materials are very different [3, 4]. On the atomic scale, the occupational defects are often randomly distributed, resulting in a reduction of the degree of ordering [5]. These defects can also exist on a larger scale, leading to antiphase domains [5, 6]. The domain structure alters the phase of the scattered x-rays and consequently the peak position and intensity. Let us consider that an ideal 1/1 superlattice with correct sequence {ABABAB....AB} becomes {ABAB...AB|BABA...BA} with an antiphase boundary. The x-ray intensity of (00l) reflection changes from

$$I = \text{const} \cdot |F_{\text{AB}}|^2 \frac{\sin^2 2\pi Nl}{\sin^2 \pi l} \tag{5}$$

to

$$I = \text{const} \cdot |F_{\text{AB}}|^2 \frac{\sin^2 \pi Nl}{\sin^2 \pi l}[1 - \cos 2\pi Nl], \tag{6}$$

where F_{AB} is the structure factor of an AB pair and N is the size of the antiphase domain. Equation (5) results in correct (003)

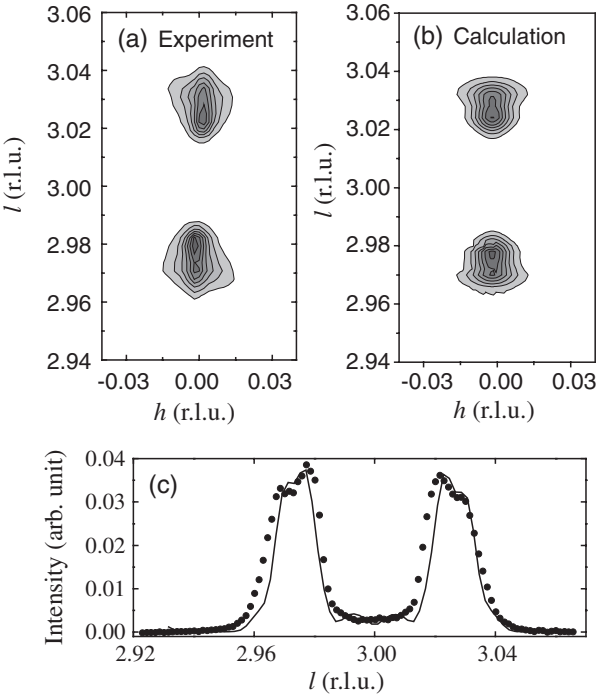

Figure 8. (*a*) Measured and (*b*) calculated x-ray intensity contour maps around the (003) reciprocal lattice point of the 1/1 superlattice with a 10 s growth interruption after deposition of each ML. (*c*) l-scan at $h = 0$. The dots and line represent the measured and calculated results, respectively.

peaks at $l = 3$, whereas equation (6) results in two split peaks located at $l = 3 \pm 1/2N$, as shown in figure 9. Therefore, the splitting of the (003) peak in figures 2(*a*) and (*b*) suggests that there are 'antiphase boundaries' in the growth direction. The extra peaks seen from the 4/4 superlattice (figure 3(*a*)) also suggest that there is an additional triple-period modulation in the same direction. In addition, the randomly distributed lateral antiphase domains can cause the broadening of the diffraction peaks [5, 7]. Thus, we consider a structural model shown in figure 10 for our superlattices. In other words, the superlattices are composed of alternating overall GaAs-rich and AlAs-rich layers. Within each layer, there are also GaAs-rich and AlAs-rich domains. From the experimental results of 1/1, 2/2 and 4/4 superlattices, as noted above, the vertical extent of the lateral domains is just about 1–2 MLs.

We denote the three crystal axes as $\boldsymbol{a}$||[100], $\boldsymbol{b}$||[010] and $\boldsymbol{c}$||[001], respectively, where the superlattice was deposited along the $\boldsymbol{c}$-axis. The domain boundaries in figure 8 can then be attributed to half diagonal and full diagonal glides involving displacements $(\boldsymbol{b} + \boldsymbol{c})/2$ and $(\boldsymbol{b} + \boldsymbol{c})$ across planes perpendicular to the $\boldsymbol{a}$-axis and displacements $(\boldsymbol{a} + \boldsymbol{c})/2$ and $(\boldsymbol{a}+\boldsymbol{c})$ across planes perpendicular to the $\boldsymbol{b}$-axis. If γ represents the possibility of crossing a domain boundary at a distance a, where a is the unit cell dimension of cubic GaAs, a/γ is the average size of the in-plane domains.

The structure factor of the mth pair of MLs containing lateral domains can be written as [8]

$$F_{2D,m} = F_m \cdot G, \tag{7}$$

where F_m is the structure factor of the mth pair of MLs of the perfectly ordered structure. G is a factor accounting for

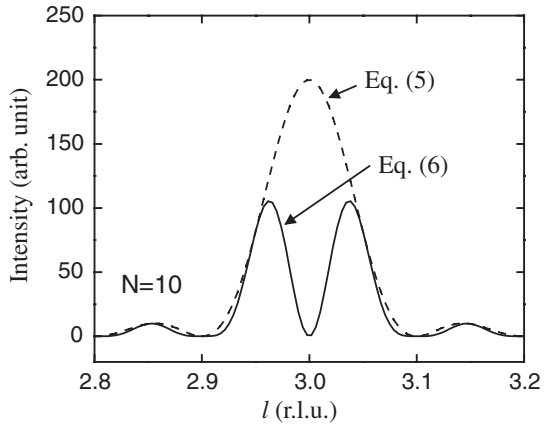

Figure 9. Calculated x-ray (003) l-scan for a 1/1 structure with (——) and without (- - - -) an antiphase boundary.

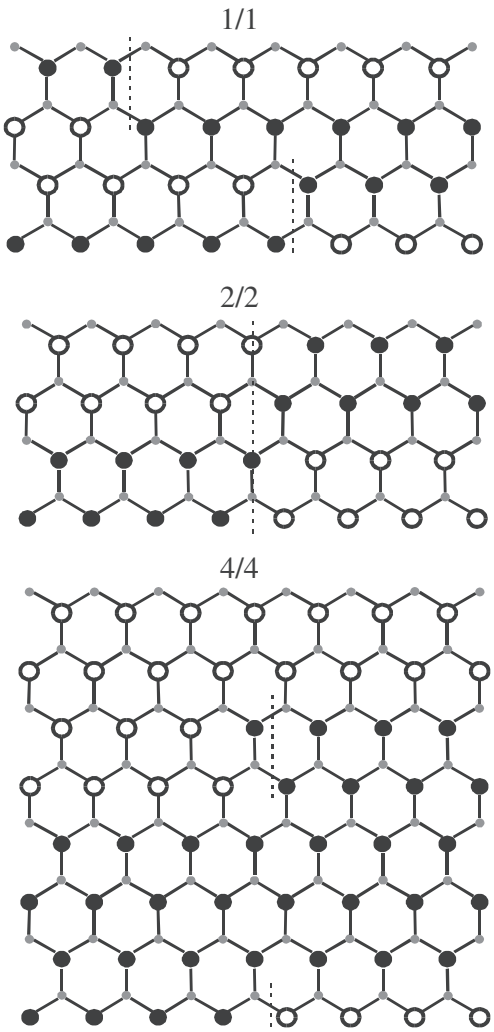

Figure 10. Schematic diagrams presenting the lateral antiphase domain structure in the 1/1, 2/2 and 4/4 superlattices.

the lateral domains. G for reflection (hkl) can be written in the form [3]

$$G = \sum_{n_1}\sum_{n_2}\langle e^{i\phi(1)}\rangle^{|n_1|}\langle e^{i\phi(2)}\rangle^{|n_2|}e^{2\pi i n_1 h}e^{2\pi i n_2 k}, \qquad (8)$$

where $\langle e^{i\phi(1)}\rangle$ and $\langle e^{i\phi(2)}\rangle$ denote an average phase shift across a unit cell boundary in the in-plane [100] and [010] directions, respectively, which for simplicity can be assumed the same. n_i ($i = 1, 2$) is the distance between any two cells in the [100] and [010] directions, respectively. In our experiment, we have taken $h = k$, so that the average phase factor is

$$\langle e^{i\phi(1)}\rangle = \langle e^{i\phi(2)}\rangle = \eta = \begin{cases} 1-\gamma+\gamma e^{i\pi(h+l)} & \text{for 1/1,} \\ 1-\gamma+\dfrac{\gamma[e^{i\pi(h+l)}+e^{i\pi(h-l)}+e^{i2\pi(h+l)}+e^{i2\pi(h-l)}]}{4} & \text{for others.} \end{cases} \qquad (9)$$

Here, we have assumed the same probability for the 1 and 2 ML perturbations. The G factor now becomes

$$G = 1 + \frac{\eta e^{2\pi i h}}{1-\eta e^{2\pi i h}} + \frac{\eta e^{-2\pi i h}}{1-\eta e^{-2\pi i h}}. \qquad (10)$$

The x-ray intensity is then expressed as

$$I \propto \sum_m \sum_{m'} F_{2D,m}\cdot F^*_{2D,m'} e^{2\pi i(m-m')l}. \qquad (11)$$

To evaluate equation (11), we need to consider the vertical phase shift. The reason why the vertical phase shift can occur is that precise control of the MBE growth rate of a heterostructure is almost impossible, as revealed, for example, by the phase shift of the RHEED oscillations at the heterointerfaces [9, 10]. There is always an intrinsic small growth mistake which leads to a slight increase or decrease of deposited materials. Accumulation of these mistakes can result in periodic CSFs in the multilayer stack: a certain designed GaAs-rich layer can be actually AlAs-rich, and vice versa. Such CSFs, or mistakes in stacking order, thus cause a periodic phase change in the growth direction.

If the stacking of type A and B atomic layers of our superlattices follows a 'correct' order {ABABAB...} or {AABBAABB...} or {AAAABBBB...}, equation (11) can be easily evaluated similar to equation (5). However, if there are periodic CSFs, whose wavelength is much larger than the superlattice period, the stacking sequence may become {ABAB...AB|BABA...BA|ABAB...AB...} for the 1/1 superlattice, {AABB...AABB|BAAB...BA|AABB...AA BB.....} for the 2/2 superlattice and {AAAABBBB...AAA ABBBB|BAAABBBB...AAAABBBA|AAAABBBB.....} for the 4/4 superlattice. In this case, the superlattice can be regarded as consisting of two building blocks. Equation (11) can then be evaluated by considering these two component blocks as constituents of a long wavelength superstructure superimposed on the ordinary superlattice, similar to what we have done for equation (6).

4. Simulation results and discussion

Using the above approach, we have simulated the experimental data. The calculated reciprocal space map and the h and l line scans for the 1/1 superlattice without growth interruption are shown in figure 2 together with their experimental counterparts. Good agreements have been obtained between the measured and calculated maps as well as between the

Table 1. Period of CSFs and the average size of the lateral antiphase domains near the two interfaces: GaAl-on-AlAs and AlAs-on-GaAs.

Sample	Period of CSFs (ML)	Lateral domain size (unit cell)	
		GaAs-on-AlAs	AlAs-on-GaAs
1/1	15	11	11
2/2	12	20	20
4/4	12	11	100
1/1[a]	11–14	34	34

[a] With a 10 s growth interruption.

measured and calculated line scans. The structural parameters used for these calculations are given in table 1. From our simulation, this 1/1 superlattice has periodic CSFs every 15 MLs, which are responsible for the peak splitting, and lateral antiphase domains of an average size of 11 unit cells, which are responsible for the peak broadening. We must consider that composition mixing is almost inevitable at the ML level. Therefore, it is more realistic to call the nominal GaAs (AlAs) regions GaAs (AlAs)-rich. Considering the random occupational defects, or composition mixing, due to the known phenomenon of Ga segregation and the possible contamination due to the Ga and Al background pressure in the growth chamber, we may write the layer composition as $Ga_{0.5+s/2}Al_{0.5-s/2}As$ and $Ga_{0.5-s/2}Al_{0.5+s/2}As$, respectively, where s ($0 \leqslant s \leqslant 1$) is the so-called order parameter. In this case, equation (2) has to be replaced by

$$F_{00l} = \begin{cases} f_{GaAs} + f_{AlAs} & \text{fundamental,} \\ s(f_{GaAs} - f_{AlAs}) & \text{superlattice peak.} \end{cases} \qquad (12)$$

Clearly, the fundamental reflection is not affected by composition mixing, whereas the intensity of the superlattice peaks includes the factor s^2. We can then determine s by comparing the intensities of the fundamental (002) reflection and the (0,0,3 ± 0.033) peaks. For this 1/1 superlattice, we have determined that s is about 0.1. In other words, the Ga-rich region is $Ga_{0.55}Al_{0.45}As$ and the Al-rich region is $Ga_{0.45}Al_{0.55}As$.

The calculated results for the 2/2 superlattice are shown in figures 3 and 4. Both the shape and position of the calculated peaks in reciprocal space fit quite well to the experimental ones. To compare the measured and calculated data in a more quantitative manner, calculated line scans are also shown in figures 3 and 4, in addition to the reciprocal space maps. Here, peak shifting, instead of splitting, results because the vertical phase shift does not lead to antiphasing as in the case of the 1/1 superlattice. To understand this, let us consider an ideal 2/2 superlattice of $2N$ MLs with correct sequence {AABB....AABB} becoming {AABB...AABB|BAAB...BAAB}. The latter contains two domains of size N separated by a phase boundary. The two sequences AABB and BAAB differ by a phase factor π. Therefore, the x-ray intensity of the (00l) reflection changes from

$$I = \text{const} \cdot |F_{AABB}|^2 \frac{\sin^2 4\pi Nl}{\sin^2 2\pi l}, \qquad (13)$$

of the ideal 2/2 superlattice to

$$I = \text{const} \cdot |F_{AABB}|^2 \frac{\sin^2 2\pi Nl}{\sin^2 2\pi l}[1 + \cos(4N+1)\pi l]. \qquad (14)$$

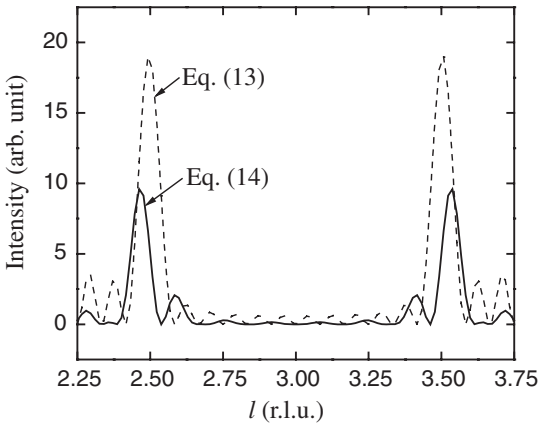

Figure 11. Calculated (00l) spectrum for a 2/2 superlattice with (——) and without (- - - -) an antiphase boundary using equations (14) and (13) by taking $N = 3$.

Like equation (6), the term in the bracket has maxima when $(4N+1)l$ is an odd number. This thus causes peak shifts at positions where $l = m/2$ (m is odd). The results calculated using equations (13) and (14) by taking $N = 3$ are shown in figure 11. Clearly, the phase shift causes the shift in the peak position in a different manner at different l. By simulating the experimental data, we have determined that the period of the CSFs is about 12 MLs and the average lateral domain size is 20 unit cells. The average order parameter, s, for the 2 MLs of the same material is 0.15, slightly higher than in the 1/1 superlattice.

The 4/4 superlattice is more complicated. In order to fit the l-scan shown in figure 5, we have first assumed that there is a periodic CSF approximately every 12 MLs, resulting in the extra peaks between the superlattice reflections. These CSFs have imposed an additional long wavelength modulation three times greater than the superlattice period. Then, as discussed in equation (4), we also have to assume that there is a composition change between the first two MLs and the next two MLs of the same material in order to produce non-vanishing (0,0,m/2) ($m = 3$ and 5) peaks. As for the h-scans (figures 5(b) and (c)), the two-component profiles are obtained by considering that the domain structure is asymmetric; i.e. the lateral domains in the top two and the bottom two MLs of the same material, either GaAs-rich or AlAs-rich, do not have the same size. Specifically, because of the low mobility of the Al atoms, we have assumed that the domains near the GaAs-on-AlAs interfaces are smaller than those near the AlAs-on-GaAs interfaces. The calculated results agree very well with the experimental curves in figures 5(b) and (c). From the calculations, we determined that the narrow component corresponds to large domains of about 100 unit cells near the AlAs-on-GaAs interfaces, whereas the broad component corresponds to small domains of about 11 unit cells near the GaAs-on-AlAs interfaces. Again, as mentioned earlier in our discussion of the experimental results, the fact that the asymmetric interfacial structure is observed in the 4/4 superlattice but not in the 1/1 and 2/2 superlattices is a clear indication that the lateral domain structures extend no more than 2 MLs in the vertical direction.

With the further increase in the superlattice period, the volume fraction of the 2 ML domain structure near the

interfaces decreases and so does the x-ray signal from them in the diffraction pattern, as show by the 10/10 superlattice (figure 6). No CSFs are expected for this sample because the superlattice period is larger than the possible CSF period of about 12 MLs, as determined earlier. Therefore, the growth error will only accumulate composition variation, or roughness, at the interfaces. With an abrupt interface model, we calculated the (002) l-scan, as shown in figure 6. It agrees quite well with the experimental data, indicating that large angle diffraction is not sensitive to this roughness. The transverse scan at the first order superlattice peak, shown in figure 7, is very narrow, but the trace of a broad component, as shown by the dashed line, is still visible, indicating the existence of lateral domains at the interfaces.

Now, let us consider the 1/1 superlattice with a 10 s growth interruption. The lateral width of the peaks is now much narrower than that of the 1/1 superlattice without growth interruption (figure 8). To fit these data, we have assumed an average lateral domain size of 34 unit cells. This indicates that during the growth interruption, the lateral domains grow due to increased time for atoms to migrate on the surface. The shoulders in the l-scan of this sample are likely due to the changes in the CSF period. We obtained a fit by considering that the spacing between the CSFs has changed from 14 MLs in the lower part of the structure to 11 MLs in the upper part. The agreement between measurement and calculation is good except that the calculated l-scan is narrower than the measured one. We believe that this discrepancy is probably because the CSF spacing actually varies randomly between 11 and 14 MLs and this random variation is not considered in our calculation.

The existence of the CSFs in the growth direction has been confirmed by high-resolution transmission electron microscopic (HR-TEM) experiments after our x-ray measurements. In an earlier study of the AlAs/GaAs atomic-layer superlattices, a missing ML seems to have been observed by cross-sectional scanning tunnelling microscopic (XSTM) experiments, but no explanation was given [11, 12]. Such a missing ML is what we have now regarded as a CSF due to the growth rate error. In our samples, the CSFs have a period of 12–15 MLs, equivalent to an growth rate error of about 5–8%. It is also worth pointing out that with XSTM, a structure smaller than the 4/2 superlattice cannot be distinguished from random AlGaAs alloys due to small sampling area and bad statistics [11, 12]. Our x-ray experiments, however, are able to observe the ordered structure in a structure as small as a 1/1 superlattice because, by their nature, they average over a macroscopic region.

5. Conclusion

We have characterized the structure of AlAs/GaAs atomic-layer superlattices. A lateral domain structure of vertical extent of about 2 MLs has been observed in our samples. In addition, periodic CSFs form in the growth direction due to small growth rate errors. We have shown that a conventional x-ray kinematic diffraction technique is quite useful for the characterization of these atomic layer structures.

Acknowledgments

We thank Drs Pfeiffer and West of Bell Laboratories for providing the samples. The work is supported by NSF DMR-0408539 and the State of Texas through the Texas Government through the Texas Center for Superconductivity and Advanced Materials at the University of Houston.

References

[1] Holy V, Pietsch U and Baumbach T 1999 *High-Resolution X-ray Scattering from Thin Films and Multilayers* (Berlin: Springer)
[2] Sinha S K, Sirota E B, Garoff S and Stanley H B 1988 *Phys. Rev.* B **38** 2297
[3] Warren B E 1990 *X-ray Diffraction* (New York: Dover)
[4] Mascarenhas A 2002 *Spontaneous Ordering in Semiconductor Alloys* (New York: Kluwer)
[5] Li J H, Kulik J, Holy V, Zhong Z, Moss S C, Zhang Y, Mascarenhas A and Bai J 2001 *Phys. Rev.* B **63** 155310
[6] Zhong Z, Li J H, Kulik J, Chow P C, Norman A G, Mascarenhas A, Bai J, Golding T D and Moss S C 2001 *Phys. Rev.* B **63** 33314
[7] Zhong Z, Holy V, Li J H, Kulik J, Bai J, Golding T D and Moss S C 2001 *J. Appl. Phys.* **90** 644
[8] Li J H, Moss S C, Zhang Y, Mascarenhas A, Pfeiffer L N, West K W, Ge W K and Bai J 2003 *Phys. Rev. Lett.* **91** 106103
[9] Braun W and Ploog K H 1993 *J. Appl. Phys.* **75** 1993
[10] Braun W, Trampert A, Daweritz L and Ploog K H 1997 *Phys. Rev.* B **55** 1689
[11] Smith A R, Chao K-J, Shih C K, Shih Y C, Anselm K A and Streetman B G 1995 *J. Vac. Sci. Technol.* B **13** 1824
[12] Smith A R, Chao K-J, Shih C K, Shih Y C and Streetman B G 1995 *Appl. Phys. Lett.* **66** 478